Superfluidity and film structure in ^{4}He adsorbed on graphite

P. A. Crowell* and J. D. Reppy
Laboratory of Atomic and Solid State Physics and Materials Science Center, Clark Hall, Cornell University, Ithaca, New York 14853-2501
(Received 18 July 1995)

We have completed a torsional-oscillator study of superfluidity in thin films of ^{4}He adsorbed on the basal plane of graphite for coverages from $1\frac{1}{2}$ to 7 atomic layers. In contrast to superfluidity in films adsorbed on amorphous substrates, we find several different regimes of superfluid behavior. Superfluidity in the second layer shows an anomalous temperature dependence and is destroyed by solidification of the film. The superfluid film appears to coexist with a two-dimensional surface gas for low coverages in the third layer. Evidence of a phase transition, which may be the reconstruction of an underlying layer, appears just above the completion of the third layer. Modulation of the superfluid signal with coverage is seen through the completion of the sixth layer.

I. INTRODUCTION

Thin films of ^{4}He have played an important role in studies of both superfluidity and the growth of films on surfaces. In the case of superfluidity, the reduced dimensionality leads to a realization of the Kosterlitz-Thouless transition predicted for two-dimensional (2D) systems with a broken continuous symmetry.[1,2] On the other hand, the growth of ^{4}He films adsorbed on substrates such as the basal plane of graphite is characterized by a rich structural phase diagram which has provided considerable insight into the thermodynamics of low-dimensional quantum systems.[3,4] In spite of the progress made in both of these areas, the relationship between superfluidity and film structure remains poorly understood. With few exceptions, studies of thin-film superfluidity have been confined to amorphous substrates,[5–7] on which ^{4}He films show no evidence of the layer-by-layer growth observed on graphite, which is ordered on atomic length scales.[3,8] The smooth and monotonic development of superfluidity with coverage in the experiments on amorphous substrates has pushed structural considerations into the background.

In this paper, we report measurements that demonstrate the influence of film structure on superfluidity in the case of ^{4}He adsorbed on the basal plane of graphite. Using the torsional oscillator technique, we have completed a systematic study of the superfluid mass for coverages between $1\frac{1}{2}$ and 7 atomic layers and temperatures between 20 mK and 1.2 K. We find that the evolution of superfluidity with increasing coverage is very different from that found on amorphous substrates. In the second layer of adsorbed ^{4}He, superfluidity is destroyed by solidification of the film. We find evidence that the superfluid film coexists with a 2D surface gas over part of the third layer. The growth of superfluidity is entirely suppressed just above third-layer completion and is partially suppressed near the completion of the fourth through sixth layers.

This paper provides a comprehensive discussion of our studies of the ^{4}He-graphite system.[9] Since our results do not address any particular theory or set of predictions, the appoach adopted here is predominantly phenomenological. Section II reviews the structure of ^{4}He films on graphite, with emphasis on two-phase coexistence, which we believe determines some of the unusual superfluid properties of this system. Experimental details particular to our measurements are discussed in Sec. III. The next three sections review and discuss the results for different coverage ranges: the second layer of adsorbed ^{4}He, the third and fourth layers, and coverages beyond four layers. Before concluding, we will discuss briefly the outlook for the first one and one-half layers, which we have not yet studied in detail. Within the resolution of our measurements, we do not observe superfluidity in this regime.

II. ^{4}He FILMS ADSORBED ON GRAPHITE: BACKGROUND

Information about the structure of ^{4}He films adsorbed on graphite has been derived in large part from heat capacity,[3,4] neutron scattering,[10] and chemical potential measurements.[11] The most important fact to note about the growth of ^{4}He films on graphite is that it occurs in a *layer-by-layer* fashion out to at least seven layers.[8] In this context, *layer-by-layer* means that the chemical potential μ at low temperature shows steplike behavior as a function of coverage. μ is nearly constant while a layer is being filled but increases rapidly near completion due to the strong He-He repulsion. It is then energetically favorable for additional He atoms to occupy the next layer. We emphasize that this layer-by-layer growth is very different from that found on amorphous substrates such as glass, for which the chemical potential grows smoothly, approximately as $1/n^3$, with increasing coverage n. In the case of ^{4}He-graphite, the size of the chemical potential step is approximately 15 K between the second and third layers and 5 K between the third and fourth layers.[12] (The steps are typically smeared out over a fraction of a layer. This may be due to the presence of adsorption sites at step edges and other defects of the exfoliated substrates used in most experiments.)

A. Phase diagram of ^{4}He films on graphite

The phase diagram of ^{4}He films on graphite continues to be the subject of both experimental and theoretical

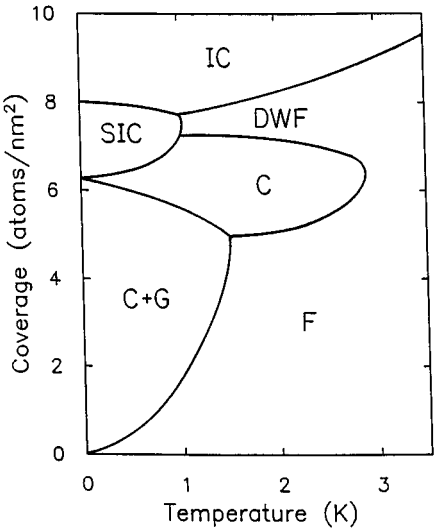

FIG. 1. The phase diagram of the first layer of ^{4}He adsorbed on the basal plane of graphite (Ref. 15). The high-temperature fluid phase is labeled F. The phase labeled C is the commensurate solid. The commensurate solid and a 2D surface gas coexist in the region $C+G$. The layer forms a hexagonal close-packed incommensurate solid (IC) above 8 atoms/nm^2 at $T=0$. The remaining phases are a striped incommensurate solid (SIC) and a domain-wall fluid (DWF). The second layer begins to fill at 12 atoms/nm^2.

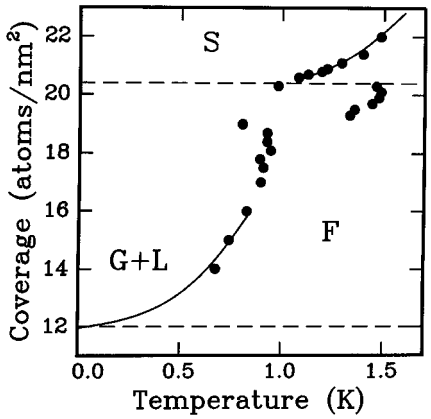

FIG. 2. The phase diagram of the second layer of ^{4}He on graphite following Polanco and Bretz (Ref. 17) is shown using solid curves. $G+L$, F, and S indicate the gas-liquid coexistence region, the uniform fluid phase, and the second-layer incommensurate solid. The points show the loci of heat capacity peaks from the study of Greywall and Busch (Ref. 12). The dashed lines indicate promotion to the second and third layers.

investigation.[4,13] Since extensive reviews of the field are available,[14] we will focus here on the aspects which may be relevant for our study of superfluidity.

The accepted phase diagram for the first layer of ^{4}He adsorbed on the basal plane of graphite is shown in Fig. 1.[15] The salient features of this phase diagram at low temperatures are the commensurate solid-surface gas coexistence region ($C+G$) at low coverage, the commensurate solid (C) at intermediate coverage, and the incommensurate solid (IC) for coverages above 8 atoms/nm^2.[3] The remaining phases are a striped incommensurate solid[16] (SIC) and the domain-wall fluid (DWF) in the transition region between the C and IC solid phases.

The second layer of ^{4}He on graphite has been studied in less detail. Measurements of Polanco and Bretz[17] indicate a two-phase coexistence region at low coverages. Because of the reduced attraction to the substrate, the coexisting phases are thought to be a 2D liquid and a surface gas as opposed to the gas-solid coexistence favored for the first layer. Bretz[18] found a line of heat capacity peaks, which he associated with the melting of the second-layer solid, starting at coverages just above the start of the third layer. The coexistence region ($G+L$) and the second-layer solid (S) are indicated in Fig. 2. Phase boundaries following from the study of Polanco and Bretz are shown using solid curves.

Greywall and Busch (GB) have recently completed a detailed heat capacity study of the first and second layers of adsorbed ^{4}He.[4,12] Within the first layer, their data are generally consistent with those of previous studies. We superimpose a map locating the position of peaks in their second-layer data on the phase diagram of Fig. 2. The line of heat capacity peaks at low coverages follows that of Polanco and Bretz, and GB also find the melting peak above second-layer completion. In addition, however, they find a line of peaks, between 19 and 20.5 atoms/nm^2 in Fig. 2, which they associate with the melting of a second-layer registered solid. GB propose that this solid is commensurate with the first-layer incommensurate solid, with a $\sqrt{7}\times\sqrt{7}$ structure identical to that suggested earlier for one of the second-layer phases of ^{3}He.[19] Although this structure cannot be verified at this time, the data shown in Fig. 2 suggest strongly that the second layer solidifies *before* completion.

The existence of well-defined 2D phases for the third and higher layers is unresolved. GB find a line of heat capacity peaks for low third-layer densities which they associate with a gas-liquid coexistence region similar to that seen in the second layer. Data for higher layers are dominated by a large background due to the heat capacity of the second-layer solid and are inconclusive.

B. Two-phase coexistence

We now turn to the low-density regions of the phase diagram for each of the first three layers. Two-phase coexistence of some sort is believed to occur in each case. The primary evidence for this is a line of heat capacity peaks seen in the relevant coverage regime of each layer. The conventional interpretation is that this line traces the first-order phase boundary between the coexistence region and a uniform fluid phase. The jump discontinuity in the specific heat expected for such a boundary is presumed to be rounded by substrate heterogeneity and excitations in the liquid, leading to the rounded peak observed experimentally.

Greywall and Busch[12] adopt a different approach and have conducted a detailed analysis based on their heat capacity isotherms as a function of coverage. They note that for an ideal system, the isothermal heat capacity within a coexistence region should vary linearly with density,[20] and their analysis leads to a phase diagram for the first layer that is significantly different from the conventional one shown in Fig. 1. GB argue that a 2D liquid coexists with a surface gas

up to a coverage of 4 atoms/nm^2 at $T=0$ and that the commensurate solid coexists with a 2D liquid until perfect registry is reached at $n=6.37$ atoms/nm^2. They also argue for the existence of gas-liquid coexistence regions approximately 4 atoms/nm^2 wide for low coverages in the second and third layers. In each case, the boundary of the proposed coexistence region does not follow the traditional map of heat capacity peaks. Although there is no reason *a priori* why a heat capacity peak must indicate a phase transition, we note that the tricritical point where the $C+G$ phase boundary meets the pure C phase in Fig. 1 is well documented,[21] but is absent in the GB phase diagram. We are therefore reluctant to reject the traditional picture of the first layer. Nevertheless, the proposal of Greywall and Busch raises two interesting points. First, what is the nature of the two-phase region, and why should it be different in the first layer than in the higher layers, where the condensed phase is assumed to be a liquid? Second, what alternative explanations exist for the heat capacity peak normally associated with the boundary of the two-phase region?

The first of these questions has been addressed in a variety of theoretical studies. Whitlock *et al.* considered an ideal helium film confined to two dimensions in the absence of a substrate.[22] They showed that the film is a self-bound liquid at $T=0$ with a density n_0 of 4 atoms/nm^2, meaning that films of areal density less than n_0 should condense into 2D liquid droplets at $T=0$. This result thus implies a gas-liquid coexistence region at low temperatures for densities below 4 atoms/nm^2. The film is a uniform fluid at $T=0$ for higher densities.

The first layer of ^{4}He on graphite is a poor system for applying the model of Whitlock *et al.* The substrate potential, which is ignored in their calculation, is clearly important given the rich phase diagram. Furthermore, the existence of a commensurate solid indicates that a realistic potential must include the in-plane corrugation as well as the average van der Waals attraction for the adsorbate. Using a realistic substrate potential, Gottlieb and Bruch[23] have compared the binding energies of the 2D liquid and the commensurate solid. Their most recent calculation finds that the liquid is more strongly bound than the solid, lending some support to the proposal of Greywall and Busch.

For the second and higher layers, one would expect that the approximation of an ideal ^{4}He film should be more appropriate, since the lateral corrugation due to the substrate is much weaker than in the first layer. The van der Waals attraction, however, is still present. Clements *et al.*[13] have attempted to address this by studying multilayer ^{4}He films on a smooth ''pseudosubstrate'' comprising two solid layers of ^{4}He on graphite. This calculation predicts that the third layer, which is the first fluid layer in their model, will condense into self-bound 2D droplets with a density of 3.5 atoms/nm^2. Furthermore, the multilayer calculation indicates that phase separation will also occur in the layers *above* the first fluid layer out to at least the third fluid layer.

There is thus much theoretical work indicating gas-liquid coexistence in ^{4}He films. As discussed above, Greywall and Busch conclude that the phase diagrams of the first through third layers of ^{4}He on graphite should include such coexistence regions, but that they are smaller than the regions mapped out in traditional fashion by a line of heat capacity peaks. They argue further that the liquid phase in each layer should be superfluid at low enough temperature and that the line of heat capacity peaks previously associated with the boundary of the coexistence region is in fact a signature of superfluidity. The peak in this case is presumed to be that expected for a Kosterlitz-Thouless (KT) transition in a 2D superfluid,[24] and GB show that their heat capacity data for densities near 4 atoms/nm^2 are in reasonable agreement with the calculation of Ceperley and Pollock[25] for the heat capacity of a uniform film of density 4.3 atoms/nm^2.

Since a phase-separated film is broken up into 2D droplets, it is not evident that the KT peak should be observable, as finite-size effects should broaden it considerably. Furthermore, the heat capacity data show only a single low-temperature peak in the coverage regimes in question. The argument of GB, however, leads us to expect two peaks as a function of temperature for coverages below 4 atoms/nm^2: one due to phase separation and a second associated with the superfluid transition. GB speculate that the two phase transitions may occur simultaneously. This is possible in the case that the coexistence curve bounding the two-phase region follows a path of nearly constant temperature, but we note that the heat capacity peak for a uniform film is expected to occur at a temperature approximately 50% above the Kosterlitz-Thouless transition temperature.[24] We thus find that the heat capacity data by themselves do not make a convincing case for the existence of a phase-separated superfluid film. It is reasonable, however, to ask if superfluidity can be detected independently, perhaps by looking for superflow. This was one of the questions which led us to conduct the experiment discussed in this paper.

C. Superfluidity

In contrast to the extensive work on the structure and thermodynamic properties of ^{4}He films on graphite, superfluidity has received much less attention. The first study of superfluidity in the ^{4}He-graphite system was the mass-flow measurement of Herb and Dash.[26] Polanco and Bretz[27] adopted a thermal conductance technique, which relied on mass transport in the vapor phase and was therefore feasible only for temperatures above 1 K and coverages above three atomic layers.

Historically, the most fruitful technique for the study of superfluidity in the ^{4}He-graphite system has been third sound, which is a capillary wave of the superfluid film.[28] A series of dips, periodic in coverage with a period of one layer, occurs in the third sound velocity measured on graphite as the coverage is increased above three atomic layers.[8,29] The dips correspond to an acoustical softening of the film. Zimmerli *et al.*[8] have demonstrated that this softening is slightly offset from the maximum in the thermodynamic compressibility determined from vapor pressure isotherms. Unfortunately, the third sound signal is strongly attenuated for coverages below about 3.3 layers, and so these measurements could not be extended to lower densities.

Since the third sound data fall entirely in the regime in which the third sound velocity is *decreasing* as a function of increasing coverage,[28] they imply an onset coverage for superfluidity of three layers or smaller. We note that superfluidity in either the second or third layers of ^{4}He on graphite

would occur under ideal circumstances: a single layer of ^{4}He on top of a crystalline ^{4}He substrate. Superfluidity in the first layer would be even more interesting since it would occur only in the presence of the ordered, but strongly corrugated, graphite substrate. As discussed above, heat capacity measurements[3,12] indicate rich structural phase diagrams for both the first and second layers and a possible gas-liquid coexistence region in the third layer. As a result, superfluidity in any one of the first three layers is likely to be influenced by structural phase transitions.

III. EXPERIMENTAL DETAILS

The superfluid density measurements discussed in this paper were conducted using the torsional oscillator technique, which has been reviewed in detail elsewhere.[7,30] The use of exfoliated graphite substrates leads to a few special design considerations that we will discuss here. First, the exfoliation process creates a tortuous path for superflow, resulting in a very small experimental signal. Second, some *in situ* probe is necessary to establish that the substrate is clean and to measure its surface area.

A. Substrates

Our experiments used two substrates, Grafoil and UCAR graphite foam.[31] Both are manufactured by the chemical exfoliation of natural graphite. Grafoil is subsequently pressed into sheets 0.25 mm thick. The high surface areas of these substrates ($\sim$ 25 m^2/g) comes at a cost: The regions of crystalline order are small, on the order of 800–1000 Å for graphite foam and 100–200 Å for Grafoil.[32] Furthermore, there are steps, cracks, and dead ends which reduce the connectivity of the substrate. Optical investigation of both substrates shows that the largest particle size is on the order of 10 μm.

The relatively poor connectivity on macroscopic length scales has significant consequences for the torsional oscillator measurements. A torsional oscillator measures the superfluid mass that is decoupled from the substrate. For ideal superflow on a flat surface, the measured superfluid density at $T=0$ is simply the areal density of the film (after a correction for the nonsuperfluid coverage, which is typically about two monolayers). In practice, the signal is always smaller than the ideal value, since the superfluid has to flow past obstacles on the surface and therefore imparts momentum to the substrate. The fraction of the superfluid momentum transferred to the substrate in this manner is denoted the *tortuosity factor* χ. For Mylar, which has been used for many studies of the Kosterlitz-Thouless transition in ^{4}He films, $\chi \approx 0.14$.[7]

An estimate of the tortuosity factor for exfoliated graphites can be determined from the relation[33]

$$n = \frac{1}{\sqrt{1-\chi}}, \tag{1}$$

where n is the index of refraction for the appropriate sound mode, which is fourth sound[34] for full-pore ^{4}He and third sound for thin films. Roth *et al.*[35] have measured fourth sound indices of refraction of 3 and 4.5 for graphite foam and Grafoil, respectively, corresponding to tortuosities of 0.87 and 0.95. The difference between the two substrates is due mostly to the larger open volume of the foam. This distinction disappears for the case of thin films, for which the flow is restricted to the surface. The index of refraction for third sound of ^{4}He on graphite foam is 5.1 ± 0.3, giving a tortuosity factor $\chi = 0.96$.[35] Although we were not aware of a similar measurement for Grafoil, we expected the surface tortuosity to be greater than the full-pore value and thus had to allow for a superfluid signal on the order of 1% of the ideal value.

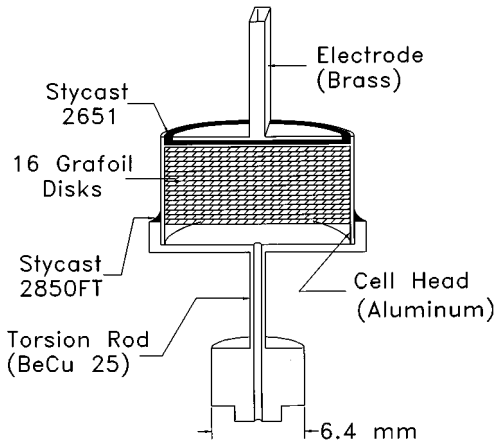

FIG. 3. A cross section of the Grafoil cell. The head is aluminum and the torsion rod is beryllium copper. The electrode structure is brass and is electrically isolated from the head by a thin layer of epoxy.

B. Experimental cell

Two experimental cells were constructed, one containing UCAR graphite foam and the other Grafoil. Almost all of the data were obtained with the Grafoil cell, and the discussion here will be limited to it. A complete review of the experimental details for both cells can be found in Ref. 36.

The design of the Grafoil cell represented a compromise between maintaining a clean substrate and obtaining a mass sensitivity good enough to compensate for the tortuosity effects. We decided to seal the cell with epoxy, thus entailing the risk of contaminating the substrate. The *in situ* characterization discussed below confirmed that the substrate was clean enough to support the layer-by-layer growth of ^{4}He films. A drawing of the cell is shown in Fig. 3. Sixteen Grafoil disks, 12.2 mm in diameter and 0.25 mm thick, were held by compression inside a thin-walled aluminum can. The Grafoil disks were heat treated for 30 minutes in an H_2 atmosphere at 900 °C before being pressed into the can, which was glued with Emerson Cumming Stycast 2850FT epoxy onto a Be-Cu 25 torsion rod, 1 mm in diameter. A brass electrode, which was isolated electrically from the remainder of the cell, was epoxied to the top of the aluminum can. The torsion rod was attached to a massive vibration isolator using a rotatable ring. The isolator was in turn mounted on the low-temperature stage of a dilution refrigerator.

C. Strain gauge

A Kapton diaphragm strain gauge for measuring the ^{4}He vapor pressure was also mounted on the experimental

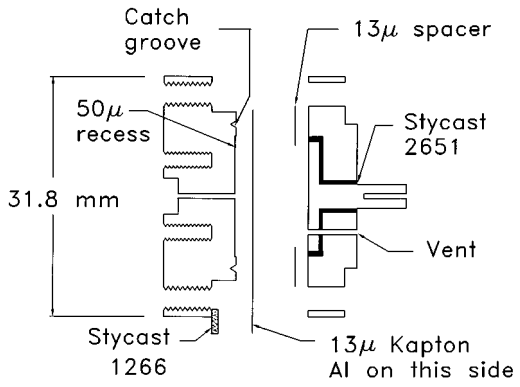

FIG. 4. An exploded cross section of the Kapton diaphragm strain gauge. The components are brass except as indicated.

stage and linked to the torsional oscillator with a capillary. The design of the gauge, which is shown in Fig. 4, is a modification of that described by Yurke.[37] We chose to use 13 μm thick Kapton foil[38] as the diaphragm. A thin film of aluminum, 2000 Å thick, was evaporated onto one side of the Kapton, which was glued to a polished brass flange with Emerson Cumming Stycast 1266 epoxy. A small recess of approximately 50 μm was machined in the diaphragm flange. The wall of this recess functioned as a stop. The diaphragm was separated from a fixed electrode of the usual insulated button design by a 13 μm Kapton spacer. The two flanges comprising the gauge were bolted together using eight 4-40 screws with spring-loaded washers. The finished gauge had a capacitance of approximately 50 pf. A calibration against the ^{4}He saturated vapor pressure indicated that the diaphragm was linear over the range ($\sim$0–20 mTorr) used in our experiments.

One drawback of the gauge was its significant hysteresis. Pressures over 10 Torr were sometimes reached when we removed helium from the cell, causing the diaphragm to short out against the fixed electrode. Upon cooling we found that the bridge ratio shifted by as much as 1%. The resulting offsets could be removed during the data analysis, but all important isotherms were conducted without subjecting the gauge to large pressures.

D. Cryogenic details

The torsional oscillator and the strain gauge were mounted on the low-temperature stage of a dilution refrigerator. Two 0.6 mm inner diameter capillaries were run from room temperature to the stage with light clamps at 4 K and the mixing chamber. The two fill lines were soldered into a block on the stage along with a capillary going to the cell and a soft-copper tube used for pumping out the cell. The absence of heat sinks prevented condensation at cold points in the fill line during the annealing process discussed below.

All of the films used in these experiments were prepared from ^{4}He drawn from a liquid helium storage Dewar. The gas was run through a helium trap and stored in a calibrated standard volume. The pressure was measured using a Baratron[39] before and after the gas was admitted to the cell. The size of the dose in μmol was determined using the ideal gas law. Since the temperature was not measured for each dose, the accuracy of this procedure was limited to about 0.5%. Extractions from the cell were conducted using the reverse of this process.

TABLE I. Annealing temperatures and cooling rates for different coverage ranges.

Coverage	Annealing temperature	Cooling rate
0–1 layers	10 K	1 K/h
1–2 layers	4 K	0.4 K/h
2–3 layers	2 K	0.2 K/h
$>$3 layers	0.9 K	0.2 K/h

After a dose of helium was admitted to the cell, it was annealed at high temperature to ensure that the coverage was uniform over the entire substrate. Although various annealing conditions were used, most coverages were annealed at the temperatures given in Table I. For coverages below three layers, we took at least 10 h to cool down the cell. At the lowest temperatures, we usually exceeded the rates given in Table I since no atoms were left in the vapor phase. Films thicker than three layers were superfluid at their annealing temperature, which facilitated the equilibration process. They were cooled more rapidly than the thinner films.

E. Surface characterization

Two of the goals of our experiment were to verify *in situ* that the graphite substrates were clean and to establish an absolute coverage scale. We chose to follow the standard practice of measuring the chemical potential of the film. If the vapor phase can be considered ideal (as is the case for the measurements under discussion here), the chemical potential μ is related to the vapor pressure P by[20]

$$\mu(T) = -k_B T \ln\left[\frac{P_0(T)}{P}\right], \tag{2}$$

where T is the temperature and $P_0(T)$ is the saturated vapor pressure. Promotion of atoms to a new layer corresponds to a step in the chemical potential at fixed temperature and hence, by Eq. (2), an increase in the vapor pressure. An adsorption isotherm taken at 900 mK for the Grafoil cell is shown in the upper panel of Fig. 5. The minimum coverage corresponds to about three atomic layers. (Steps corresponding to the completion of the lower layers were resolved only at higher temperatures.) The curve shows steplike structure through the completion of the sixth layer, indicating that the surface was not badly contaminated.

The criterion we adopt for the completion of a layer is that it occurs at the coverage n where the isothermal compressibility κ_T of the film is a minimum. The compressibility can be calculated from its definition $\kappa_T = (\partial n/\partial \mu)_{A,T}$ and Eq. (2). The compressibility calculated from the isotherm at 900 mK is shown in the lower panel of Fig. 5. From this curve, we determine that fourth-layer completion occurs at 755 ± 20 μmol. We adopt the coverage scale of Zimmerli *et al.*,[8] in which the second layer begins to fill at 12.0 atoms/nm^2 and promotion to the third layer begins at 20.4 atoms/nm^2. The density of higher layers is 7.6 atoms/nm^2.

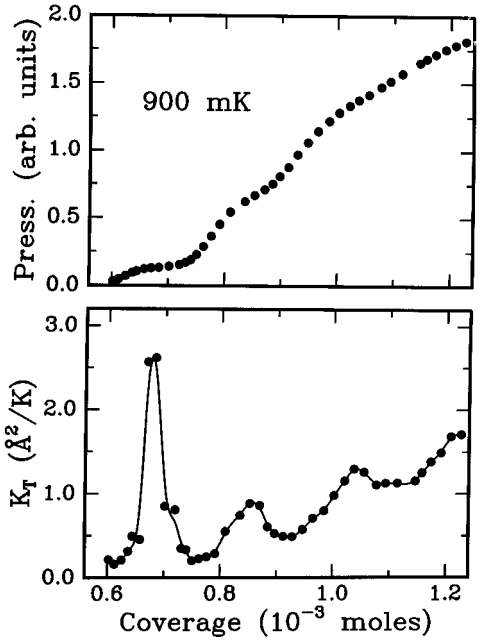

FIG. 5. Upper panel: ^{4}He adsorption isotherm on Grafoil at a temperature of 900 mK. The pressure units are arbitrary, but the maximum pressure is about 20 mTorr. Lower panel: isothermal compressibility determined from the adsorption isotherm using the procedure outlined in the text. The solid curve is a smoothed spline of the data.

Using this scale and the above value for the coverage at fourth-layer completion, we compute a surface area of 12.8 ± 0.3 m^2.

We also followed the above procedure for the graphite foam substrate used in another experimental cell and found a surface area of 2.39 ± 0.08 m^2. In this case, we were able to measure the surface area independently using the pressure step at the completion of the $\sqrt{3} \times \sqrt{3}$ registered phase in the first layer of adsorbed N_2 at a temperature of 78 K.[40] The N_2 measurement gave a surface area of 2.33 ± 0.07 m^2, which agrees within error limits with that determined from the ^{4}He vapor pressure measurements.

F. Torsional oscillator measurements

The techniques for the torsional oscillator measurements were similar to those used previously in our group.[7,30] Details pertinent to this experiment can be found in Ref. 36. The resonant frequency of the oscillator was 642 Hz and the quality factor Q of the empty cell at 4 K was 1.94×10^6. The maximum rms velocity of the substrate was between 0.2 and 0.9 mm/sec for the measurements discussed here. The oscillator was linear throughout this velocity regime and was therefore run at constant drive.

The data discussed in this paper were obtained during two experimental runs. The empty-cell period and dissipation were measured at the beginning of the second run. Instead of the empty-cell period, a ''composite'' background for the first run was constructed from the data for two nonsuperfluid films in the second layer. The period backgrounds for the two runs are shown in Fig. 6. Both are flat to within 0.02 nsec (1 part in 10^8) below 300 mK. This is rather unusual for a

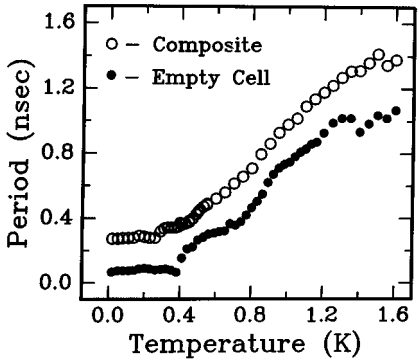

FIG. 6. The empty-cell period background for the Grafoil cell (solid circles) compared with a background constructed from two nonsuperfluid coverages in the second layer (open circles). Both sets of data have been offset by constants.

BeCu oscillator, which typically has a period minimum between 10 and 100 mK with a depth on the order of 1 part in 10^7. The flat background at low temperatures was a significant advantage of working with this cell.

The period background at higher temperatures was more pathological. The most significant feature was a step which occurred near 300 mK for the composite background and at about 400 mK for the empty-cell background, as can be seen in Fig. 6. The size of the step was different for the two backgrounds, and both the magnitude and location varied with time, making a reliable subtraction impossible. Its presence in the empty cell indicated that it was not due to ^{4}He. We found that the step was often hysteretic, occurring at a lower temperature cooling than warming. An additional, less pronounced, step occurred in the empty-cell and composite backgrounds near 700 mK and 500 mK, respectively. Both steps were accompanied by peaks in the dissipation, which, like the features in the period, varied in magnitude and position. We suspect that these features originated in a phase transition in the head of the cell, which was made from an Al alloy. The higher-temperature feature in the background, henceforth referred to as the ''500 mK feature,'' was not a significant handicap. The lower-temperature ''300 mK feature,'' however, fell in a critical region for our measurements in the second layer of adsorbed ^{4}He.

Most of the data discussed in this paper were taken in temperature sweeps. After a coverage was prepared and cooled down as described above, the temperature was incremented in steps and the resonant period and amplitude were recorded at each temperature. The mechanical ringdown time of the oscillator was so long ($\sim$20 min) that the amplitude did not always reach its equilibrium value before each measurement. For this reason, the dissipation data in this paper should be regarded as qualitative, particularly for the thicker films where the dissipation swings at the superfluid transition were very large.

The interpretation of the data for the thicker films was complicated by the desorption of atoms from the substrate at high temperatures, which resulted in a decrease in the resonant period of the oscillator. The magnitude of this effect was of the order of the superfluid signal for films thicker than four atomic layers. To correct for the desorption, we measured the resonant period and the vapor pressure at tempera-

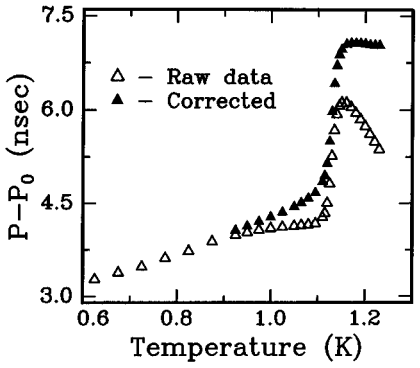

FIG. 7. Uncorrected (open triangles) and desorption-corrected (solid triangles) period data for a ^{4}He coverage of 38.2 atoms/nm^2 on Grafoil. The period offset P_0 is 1.558 84 msec.

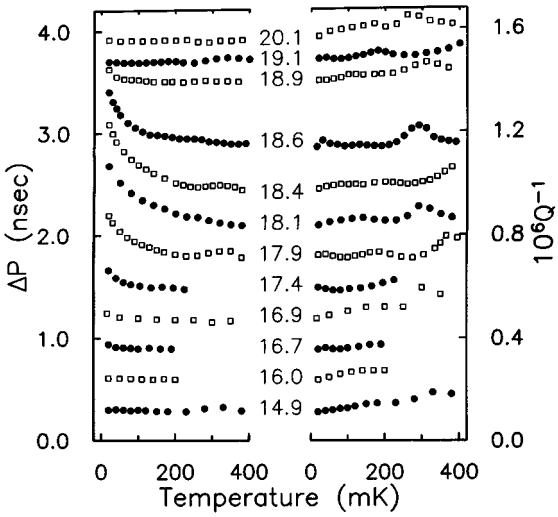

FIG. 8. Period shift (left) and dissipation (right) for ^{4}He coverages between 1.5 and 2 atomic layers. The coverage in atoms/nm^2 for each set of data is indicated at the center of the graph. The data are offset for clarity.

tures above the superfluid transition for a coverage (32.2 atoms/nm^2) at which desorption was negligible for $T<T_c$. The period was adjusted for the temperature-dependent background. Since most of the dead volume in the cell was outside the Grafoil, we assumed that the vapor was totally unlocked from the substrate, so that the drop in the resonant period as T is increased should be proportional to the mass lost through desorption and hence to the pressure. The correction factor $\alpha=\Delta(\text{period})/P$, where P is the vapor pressure, was then determined by fitting the period versus pressure data to a straight line. The vapor pressure measurements made on subsequent coverages were then used to calculate a period correction which was added to the raw data. Figure 7 shows uncorrected and corrected period data for a coverage of 38.2 atoms/nm^2.

Most of the data discussed in the following sections were obtained during temperature sweeps conducted for 50 coverages between $1\frac{1}{2}$ and $4\frac{1}{2}$ atomic layers. The resonant period and amplitude were measured at each temperature. The first step in reducing the period data was to subtract the background period from the data, after which a base line was established using the period measured at a temperature above the superfluid transition. The data were then subtracted from this base line, yielding the *superfluid period shift* $\Delta P(T)$. The low-temperature period shift $\Delta P(0)$ was determined by evaluating $\Delta P(T)$ at the lowest-temperature point, typically 20 mK. We chose this definition of $\Delta P(0)$ because it was not possible to extrapolate the period to $T=0$ for some coverages.

The dissipation was obtained from the ratio of the drive over the amplitude, which was converted to $1/Q$. Shifts in the background dissipation due to transfers as well as contamination by the 300 mK and 500 mK features made a background subtraction for the dissipation impractical. For each coverage, the dissipation data were examined for peaks associated with the superfluid transition seen in the period shift. If a superfluid dissipation peak was found, we performed a spline fit of the data near the peak. The peak temperature T_{peak} was determined by locating the zero of the derivative of the spline.

IV. SECOND LAYER

A. Results

The results of our measurements of the period shift $\Delta P(T)$ and the dissipation $1/Q$ for the second layer are shown in Fig. 8. The coverage in atoms/nm^2 is indicated for each curve. We note that the second layer begins to fill at 12.0 atoms/nm^2 and the third layer begins at 20.4 atoms/nm^2, and so the data in this figure cover the upper half of the second layer. At the lowest coverages in Fig. 8 there is no evidence of a superfluid signal. Above 17 atoms/nm^2, however, a nonzero period shift can be seen at the lowest temperatures, and it reaches a maximum at a coverage of approximately 18.4 atoms/nm^2 before falling to zero again near the completion of the second layer. There is no systematic change in the *dissipation* in this coverage regime. (Both the period and dissipation data show effects due to the 300 mK anomaly discussed above, but the features in the period are much smaller than the signal observed at lower temperatures.)

The data of Fig. 8 are unusual in several respects. First, the observed period shift is confined to a narrow region of coverage between 17 and 19 atoms/nm^2. Second, none of the data show the characteristic form for a 2D superfluid film, in which the period shift approaches some constant value as $T\rightarrow 0$. This anomalous behavior is emphasized by plotting the data on a logarithmic temperature scale, as we have done for several coverages in Fig. 9. The period is roughly linear in ln$T$ at low temperatures. Finally, although the nonzero period shift is suggestive of superfluidity, none of the curves in Fig. 8 show a well-defined transition temperature T_c. Unfortunately, contamination by the 300 mK feature prevents even a rough estimate of a characteristic temperature at which the signal vanishes for most of the coverages. The data at a coverage of 18.1 atoms/nm^2 are somewhat cleaner in this respect and seem to show a ''knee'' at a temperature of about 400 mK in Fig. 9. We emphasize,

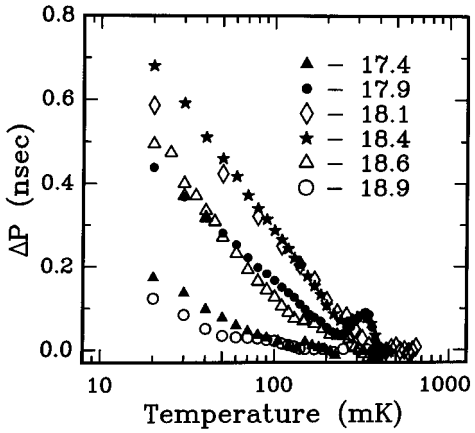

FIG. 9. The period shift ΔP for several coverages in the second layer is shown on a logarithmic temperature scale. The coverage in atoms/nm^2 for each data set is indicated in the legend.

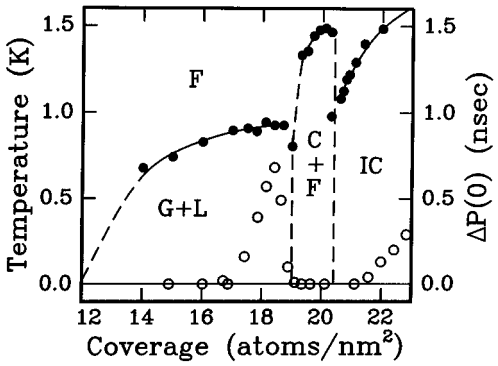

FIG. 10. A proposed phase diagram for the second layer of ^{4}He adsorbed on graphite. The gas-liquid and fluid-commensurate solid coexistence regions are labeled $G+L$ and $C+F$. F and IC indicate the fluid and incommensurate solid phases. The dashed lines indicate tentative boundaries. Promotion to the third layer occurs at 20.4 atoms/nm^2. The loci of heat capacity peaks from the study of Greywall (Ref. 4) are indicated using solid circles. The low-temperature period shift $\Delta P(0)$ from our experiment is shown (ordinate on right-hand axis) as a function of coverage using open circles.

however, that the superfluid density of a 2D film near T_c would ordinarily show a vertical drop on a logarithmic temperature scale.

We have confirmed that the observed period shift is independent of drive level for substrate velocities between 0.6 and 4 mm/sec. Since the cell had a single torsional mode, we were not able to check the frequency dependence of the effect. We did establish, however, that the effect was unchanged if the resonant period was changed slightly ($\sim$40 nsec) by adjusting the bias voltage. This test excluded the possbility that the ^{4}He coverage was somehow sweeping the cell through a parasitic resonant mode, resulting in a period shift.[6]

B. Second layer: Discussion

We believe that the period shift observed between 17 and 19 atoms/nm^2 is due to superfluidity, since it corresponds to a decrease in the effective moment of inertia of the cell. This interpretation is also consistent with the phase diagram of the second layer of ^{4}He on graphite that we deduce from the heat capacity measurements of Greywall and Busch.[4,12] In Fig. 10, we sketch this phase diagram on a map of the heat capacity peaks found in the GB study. A gas-liquid coexistence region, labeled $G+L$, exists above 12 atoms/nm^2. There remains some ambiguity about where this region terminates. In Fig. 10, the phase boundary follows the lowest line of heat capacity peaks under the assumption that these mark a first-order transition into the uniform fluid (F) phase. This line terminates close to the coverage where the line of peaks between 19 and 20 atoms/nm^2 begins. Following Greywall, we assume that this upper band of peaks corresponds to the melting of a commensurate solid, which coexists with a fluid except at the commensurate coverage. We note, however, that the isotherm-based argument of Greywall and Busch[12] leads to a smaller $G+L$ region and a correspondingly larger $C+F$ region. The peaks above 20 atoms/nm^2 correspond to the melting of the second-layer incommensurate solid IC.[18]

Figure 10 also includes the data for $\Delta P(0)$ versus coverage, which we have superposed on the map of heat capacity peaks. We first observe a nonzero $\Delta P(0)$ at a coverage of 17.4 atoms/nm^2. This coverage falls in the gas-liquid coexistence region of the phase diagram. The period shift continues to increase up to a coverage of 18.4 atoms/nm^2, above which it drops to zero again at approximately 19 atoms/nm^2. Given the proximity of the peak in $\Delta P(0)$ to the onset of solidification in Fig. 10, solidification of the film appears to be the most likely explanation for the destruction of superfluidity at higher coverages. The small gap between the maximum in $\Delta P(0)$ and the first appearance of a melting peak in the GB data are consistent with the uncertainties in the coverage scales for the two studies.

The most difficult question posed by the data in Fig. 10 is why superfluidity does not appear at a lower coverage than 17 atoms/nm^2. If we assume that the second layer of ^{4}He on graphite is an ideal 2D film, we expect that the liquid phase will be stable at a second layer density of approximately 4 atoms/nm^2, as determined by Whitlock *et al.*[22] This density corresponds to a total coverage of 16 atoms/nm^2. We emphasize that this density corresponds to the coverage at which the liquid film would cover the entire substrate uniformly. Since a network of percolating liquid patches should be sufficient to support macroscopic superflow, one would expect to see superfluidity at a lower coverage than 16 atoms/nm^2.

The merits of the percolation argument will be considered further below when we examine the third and fourth layers. It is certainly possible that the self-bound density of the liquid is higher than 4 atoms/nm^2 and/or that the naive view of percolating patches is insufficient. For some reason, the patches may not percolate until nearly the entire substrate is covered with liquid. If this is the case, only a 25% increase in the self-bound density over the theoretical prediction would suffice to explain the onset of superfluidity at 17 atoms/nm^2. The heat capacity peaks alone suggest a wider coexistence region than that found in the theoretical calculations. For example, the coexistence region that we have

sketched in Fig. 10 terminates at 19 atoms/nm^2. If this is really the case, the onset coverage of 17 atoms/nm^2 may not be so anomalous.

Before turning to the temperature dependence of the data, we consider other possible origins of the observed period shift. There has recently been renewed theoretical interest in the coexistence of superfluid order with spatial order such as that found in a solid[41] or a hexatic liquid crystal.[42] It is difficult to make a case for either of these possibilities in the absence of more detailed structural information. A superfluid state in the presence of solidlike order, sometimes referred to as a ''supersolid,'' requires the presence of zero-point vacancies in a quantum crystal.[43] In three-dimensional solid ^{4}He, there is no clear evidence for the existence of such vacancies.[44] The lower density and smaller number of nearest neighbors in a two-dimensional solid may make zero-point vacancy formation more favorable than in three dimensions, but we are not aware of any experimental evidence for their existence. Furthermore, it is not clear that a supersolid transition would actually produce a measurable period shift in a torsional oscillator experiment.

The concept of superfluidity coexisting with liquid-crystalline-like order[42] is slightly more promising. For example, a domain-wall fluid, comprising mobile stripes of helium atoms,[45] is one of the possibilities considered for the region of the first-layer phase diagram between the $\sqrt{3} \times \sqrt{3}$ commensurate solid and the incommensurate solid (see Fig. 1). Extended defects like domain walls, however, have large effective masses. Thus, even if we treat them as Bose quasiparticles, their expected Bose condensation temperature should be very low. It is likely that they would freeze into a striped incommensurate solid, as occurs in the first layer of ^{4}He-graphite, above the temperature at which they would Bose condense.

Of the above possibilities, we consider superfluidity to be the most likely origin of the period shift observed for coverages between 17 and 19 atoms/nm^2. We now turn to the unusual temperature dependence shown in Fig. 9. The most important observation concerning this figure is that the superfluid period shift continues to increase down to the lowest temperature (20 mK) used in our experiment. The data also suggest a linear relationship between ΔP and $\log_{10}(T)$ over approximately one order of magnitude in temperature. The temperature dependence is similar for coverages on both sides of the peak in $\Delta P(0)$. Figure 9 also emphasizes the lack of a clear correlation between the size of the low-temperature signal and the temperature at which the signal vanishes.

We believe that the unusual temperature dependence is due to the structure of the film. According to the argument presented above, the film is aways phase separated at the temperatures and coverages where superfluidity is present. Below the peak in $\Delta P(0)$, the two phases are a liquid and a gas, while the liquid coexists with a solid above the peak. We argue that only the liquid phases participate in superfluidity and that they actually undergo a superfluid transition at some high temperature. If the density of the liquid is on the order of 7 atoms/nm^2, we expect this transition temperature to be on the order of 1 K. The high-temperature transition is probably of the Kosterlitz-Thouless type, but it cannot be detected because the liquid regions do not form a connected path permitting superflow. We hypothesize that these liquid regions are connected by weak links which become superfluid at a sufficiently low temperature. The observed superfluid transition is tuned by these links.

There is no structural information about the nature of the links, but there are two scenarios which might lead to the observed behavior. The first of these is that the links are nearly one dimensional in character and hence have a much lower superfluid transition temperature than the 2D patches. We consider a distribution of link widths with a median width w_0, corresponding to a transition temperature of 400 mK. Imagine the superfluid patches to be points on a square lattice and the weak links to be bonds connecting them. A superfluid link will be considered a conducting bond and a nonsuperfluid link will be treated as insulating. There will be a nonzero probability that a conducting path will span the system once half the links are superfluid. This occurs at 400 mK for our proposed distribution of widths. In this crude model, we expect the superfluid period shift to increase below 400 mK in proportion to the number of superfluid paths across the system. $\Delta P(T)$ will therefore depend on the distribution of widths and the transition temperature $T_c(w)$ corresponding to a particular width.

We now consider a second proposal, in which the weak links connecting superfluid patches are all identical but have an effective conductivity that is tuned continuously by the temperature. This is the exact complement of the first theory, in which there was a wide distribution of link widths, but each link was either ''on'' or ''off.'' The origin of the unusual temperature dependence in this model is an excitation which destroys the superfluidity of each link. The theory runs into immediate difficulty, however, since we expect the number of excitations to increase with increasing temperature, which is incompatible with the concave shape of ΔP versus T. It is possible in principle to construct a density of states that would be consistent with the observed behavior, but it would have a peak at a very low energy ($E/k_B < 100$ mK), which there is no reason to expect.

Both of the models proposed here have been applied to a phase-separated system. The weak-link picture, however, may still apply even if the phase diagram of Fig. 10 is incorrect. Suppose, for example, that there is actually a uniform fluid in the coverage regime where we observe the onset of superfluidity. The connectivity of the fluid may be compromised by substrate imperfections such as steps and channels. In this case, the weak links are due to the substrate itself as opposed to being intrinsic to the phase-separated system as we have assumed above. It is possible in principle to check the importance of substrate imperfections by using a graphite substrate that has not been exfoliated. The nonexfoliated substrate will have much less surface damage. We believe that *both* phase separation and substrate geometry are relevant. If we are wrong with respect to the former, however, the nonexfoliated system should show fairly typical 2D superfluid transitions for coverages below the onset of solidification. We would also expect to detect superfluidity at a lower coverage than 17 atoms/nm^2. The suppression caused by solidification, however, should occur on both substrates.

V. THIRD AND FOURTH LAYERS

A. Results

As the third layer begins to fill at a coverage of 20.4 atoms/nm^2, we once again observe a superfluid signal. We

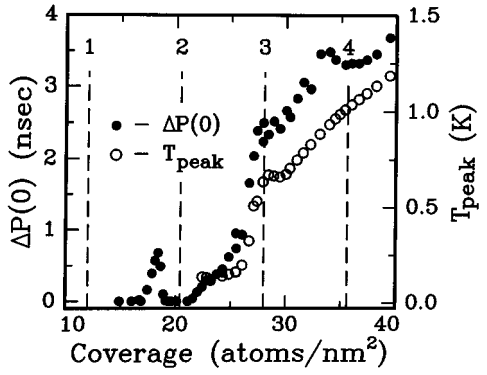

FIG. 11. The low-temperature period shift $\Delta P(0)$ (solid circles) and the temperature of the dissipation peak at the superfluid transition, T_{peak} (open circles), are shown as a function of coverage for ^{4}He films adsorbed on Grafoil. The dashed lines indicate layer completion.

also resolve a dissipation peak at the superfluid transition for coverages above 22 atoms/nm^2. Superfluidity in this coverage regime, however, continues to be unusual, as can be seen in Fig. 11, which shows $\Delta P(0)$ and T_{peak} as a function of coverage. Representative period shift and dissipation data for several coverages in the third and fourth layers are shown in Fig. 12. Figures 11 and 12 indicate several different regimes of superfluid behavior for coverages above two layers. The first corresponds to coverages between 20 and 26 atoms/

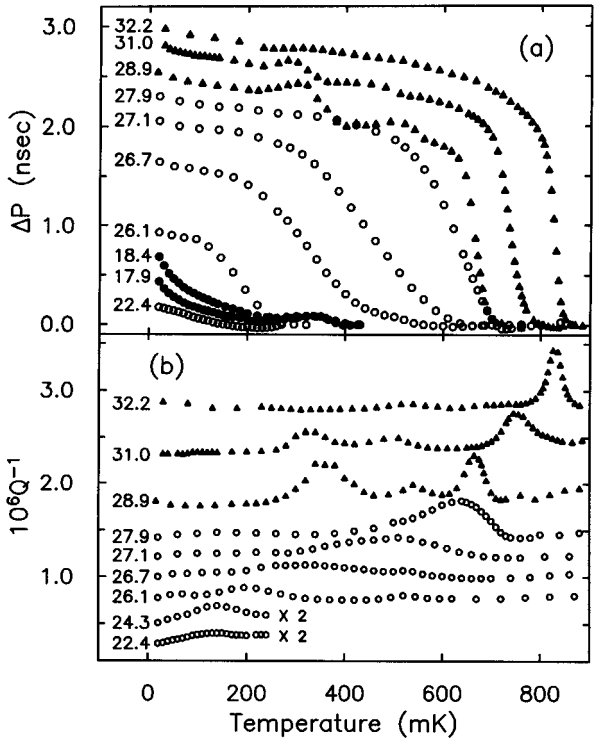

FIG. 12. The period shift (a) and dissipation (b) are shown for several coverages in the third (open circles) and fourth (triangles) layers of ^{4}He adsorbed on Grafoil. Two second-layer coverages (solid circles) are shown for comparison. The coverage in atoms/nm^2 is indicated to the left of each data set.

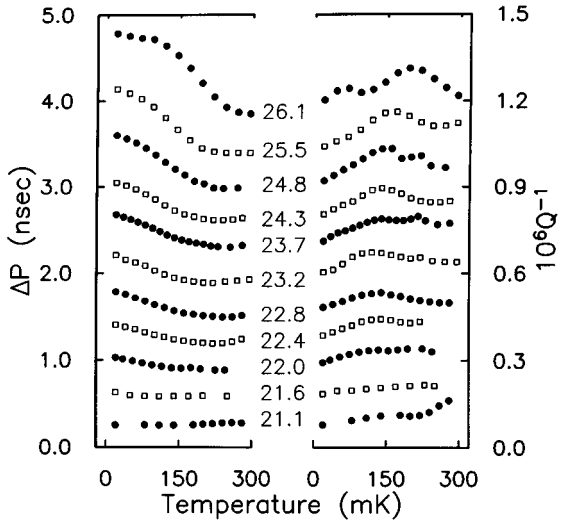

FIG. 13. Period shift (left) and dissipation (right) for coverages between 21 and 26 atoms/nm^2. The data are offset for clarity. The coverage for each set of data is given in the center of the graph.

nm^2, for which the observed superfluid transitions are very broad and the temperature T_{peak} is nearly constant. In contrast, T_{peak} increases rapidly between 26 and 28 atoms/nm^2 as the width of the superfluid transition decreases. The magnitudes of the period shift and dissipation peak also increase rapidly in this regime. Just above third-layer completion, between 28 and 30 atoms/nm^2, we observe a plateau in both T_{peak} and $\Delta P(0)$. Above 30 atoms/nm^2, the period shift and T_{peak} increase smoothly up to the vicinity of fourth-layer completion. We now review each of these coverage regimes in more detail.

1. Coverages between 20 and 26 atoms/nm^2

We first observe superfluidity in the third layer at a coverage of 21.6 atoms/nm^2, for which the period shift $\Delta P(0)$ is 0.04 nsec. This shift is comparable to the uncertainty in the background subtraction. We observe a peak in the dissipation for coverages above 22 atoms/nm^2, and the location of the maximum remains fixed at 150 ± 30 mK up to a coverage of 26 atoms/nm^2. Representative period shift and dissipation data for coverages between 20 and 26 atoms/nm^2 are shown in Fig. 13. In each case, the decrease in the period shift as T increases occurs over a range comparable to the transition temperature. Unlike the second-layer data, however, ΔP approaches a constant as $T\rightarrow0$.

As we will discuss further below, the form of the data in Fig. 13 suggests a broadened Kosterlitz-Thouless (KT) transition. In this case, the dissipation peak should occur near the superfluid transition temperature T_c. Although T_c is typically slightly below T_{peak} for a KT transition,[7] we will henceforth use T_{peak} as an estimate of T_c. If the broadening seen in Fig. 13 were due to dynamic effects, T_c could be deduced from appropriate fits to the dynamic KT theory. As we shall see below, however, the broadening is almost certainly a finite-size effect. Regardless of the microscopic mechanism of the transition, we expect that the dissipation peak should fall close to the inflection point in ΔP. Identifying the inflection points in our data was difficult since it required find-

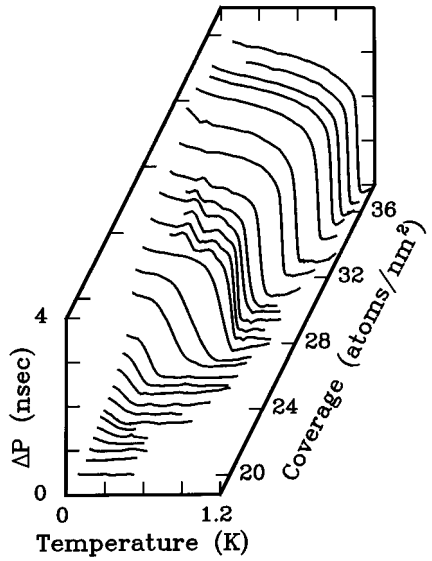

FIG. 14. Period shift data for coverages in the third and fourth layers are shown as a function of temperature and coverage.

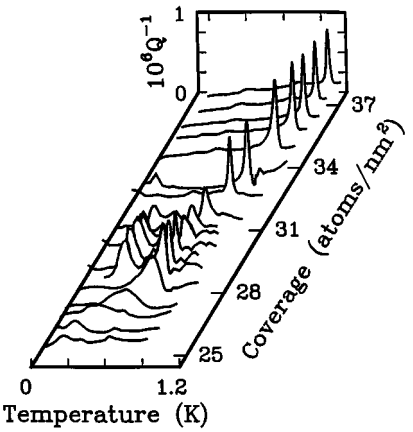

FIG. 15. Dissipation data for coverages above two atomic layers of ^{4}He adsorbed on Grafoil are shown as a function of temperature and coverage. (The scale for the dissipation is approximate.) Note the decrease in the size of the dissipation peak and the increase in width just above 30 atoms/nm^2. The line of peaks near 300 mK is not associated with superfluidity.

ing a zero in the second derivative, which was dominated by noise. Instead, we determined the temperature $T_{\rm mid}$ at which ΔP is half of $\Delta P(0)$. We found that $T_{\rm mid}$ is consistently 10–50 mK below $T_{\rm peak}$, but the two quantities have nearly the same coverage dependence, suggesting that the association of the dissipation peaks in Fig. 13 with the superfluid transition is correct.

2. Coverages between 26 and 34 atoms/nm^2

The character of the observed superfluid transitions changes as the coverage passes 26 atoms/nm^2, as can be seen in Figs. 11 and 12. The transition temperature, the period shift $\Delta P(0)$, and the size of the dissipation peak increase rapidly with coverage. The temperature dependence of both ΔP and Q^{-1} approaches the Kosterlitz-Thouless form.

Above 28 atoms/nm^2, however, the growth in $\Delta P(0)$ and $T_{\rm peak}$ suddenly stops. A plateau in both quantities occurs between 28 and 30 atoms/nm^2. The plateau in $T_{\rm peak}$ is clearly visible in Fig. 11, but the data for $\Delta P(0)$ are contaminated by noise due to the 300 mK anomaly and our failure in some cases to take data at low enough temperatures. The plateau is more apparent in a three-dimensional plot of the period shift data, which is shown in Fig. 14. The data for the coverages in the plateau region (28–30 atoms/nm^2) are nearly identical. (We do not have an explanation for why the 300 mK anomaly was so prominent in this coverage range. It did not appear on a second pass through this regime.) We have also confirmed the plateau in the period shift using the filling curve technique described below.

A composite of the dissipation data for the third and fourth layers is shown in Fig. 15, in which the plateau between 28 and 30 atoms/nm^2 appears as a line of sharp peaks near 650 mK. (The line of peaks at lower temperatures is due to the 300 mK anomaly.) As can be seen in this figure, the dissipation peak broadens and decreases in size for coverages just above 30 atoms/nm^2. We observed the same evolution of the dissipation peak with coverage for a series of films adsorbed on UCAR graphite foam.[36]

B. Third and fourth layers: Discussion

1. Third layer

The two striking features of the third-layer data are the plateau in $T_{\rm peak}$ between 22 and 26 atoms/nm^2 and the dramatic change in the character of the superfluid transition between 26 and 28 atoms/nm^2. As in the second-layer case, two-phase coexistence plays a significant role. Otherwise, the third-layer data indicate that we are dealing with a different set of phenomena. The onset of superfluidity occurs near the beginning of the layer and there is no solidification. We also resolve a dissipation peak at the superfluid transition for coverages above 22 atoms/nm^2. Perhaps the most significant difference, however, is that the temperature dependence of ΔP for the third-layer films is conventional: $\Delta P(T)$ has a meaningful low-temperature limit, and the superfluid transition appears to be a Kosterlitz-Thouless transition broadened by finite-size effects.

The third layer is the first regime in which realistic calculations of the ^{4}He film structure at zero temperature have been conducted. Clements *et al.*,[13] using a pseudosubstrate potential comprising graphite plus two solid layers of ^{4}He, find that the third-layer liquid is self-bound at a third-layer density of 3.5 atoms/nm^2, corresponding to a total density of 23.9 atoms/nm^2. Since they find no evidence of solidification of the third layer, it is reasonable to infer a third-layer phase diagram comprising a liquid-gas coexistence region at low temperatures for coverages below 24 atoms/nm^2 and a uniform fluid at higher coverages.

As shown in Fig. 11, the temperature $T_{\rm peak}$ of the superfluid dissipation peak remains fixed at 150 ± 30 mK for coverages between 22 and 26 atoms/nm^2. This observation indicates that the transition temperature T_c is nearly constant, which is reminiscent of a scenario proposed by Dash for the onset of superfluidity in a two-phase system.[46] This argument assumes that a uniform fluid of density n will undergo a superfluid transition at a transition temperature $T_c(n)$. For the purposes of our discussion, we assume that $T_c(n)$ follows the Kosterlitz-Thouless-Nelson (KTN) line.[47] Dash

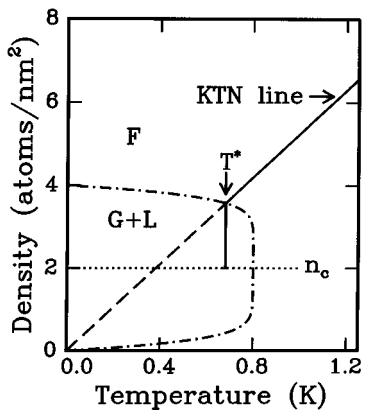

FIG. 16. A schematic representation of a case in which the KTN line passes through a gas-liquid coexistence region (adapted from Ref. 46). The two-phase coexistence region is labeled $G+L$ and the KTN line is shown as a dashed line. The actual superfluid transition temperature T_c follows the solid line, which falls on top of the KTN line in the uniform fluid phase, labeled F. The horizontal dotted line indicates the percolation threshold.

noted the possibility that the KTN line might pass through a 2D gas-liquid coexistence region as shown schematically in Fig. 16. The rest of the phase diagram is occupied by a homogeneous 2D fluid. The coexistence region ends at a density $n_0 = 4$ atoms/nm^2, the density of the self-bound liquid calculated by Whitlock *et al.*[22] (The value determined by Clements *et al.* is slightly smaller, but this only changes the width of the coexistence region.) The KTN line crosses the coexistence curve at a density n', which is slightly less than n_0. At densities less than n_0, the film will separate into two phases as it is cooled, and the density of the liquid phase n_l will increase as T decreases until $n_l > n'$. The liquid will then be superfluid. The transition temperature will therefore be fixed at $T^* = T_{\mathrm{KT}}(n')$ for *all* densities less than n'. Although the transition temperature is constant for $n < n'$, the total number of superfluid atoms varies from 0 at $n = 0$ up to An_0 at $n = n_0$, where A is the surface area of the substrate. (There is a small range $n' < n < n_0$ where superfluidity precedes phase separation as T decreases. For these densities, the amount of superfluid actually drops when the coexistence boundary is crossed.)

Although the total amount of superfluid increases as n increases from 0 to n_0, the superfluid is condensed in patches. These patches need to form a connected path across a macroscopic region in order for superfluidity to be observed in a flow measurement. The coverage at which percolation occurs depends on the size and shape of the patches. As a crude model, we consider a system of close-packed circular patches on a triangular lattice. The percolation threshold in this case occurs when the coverage is 45% of the density n_0 at which the superfluid fills the system. In a torsional oscillator experiment, we would expect to see no period shift ΔP until $n > 0.45 n_0$, above which ΔP should increase because of the greater amount of superfluid and the increase in the connectivity of the system. The superfluid transition should be broadened by finite-size effects until a uniform fluid is reached at $n = n_0$. Above this density, T_c is expected to increase with coverage according to the KTN relation, and the superfluid transition should assume the Kosterlitz-Thouless form.

The plateau in T_{peak} observed between 22 and 26 atoms/nm^2 provides some qualitative support for the percolation model. The period shift $\Delta P(0)$ increases with coverage as T_{peak} remains fixed. There are several points, however, on which agreement with the model is not very good. The plateau ends at about 26 atoms/nm^2, suggesting that the self-bound density n_0 is closer to 6 atoms/nm^2 than 4 atoms/nm^2. Furthermore, the onset of superfluidity occurs at about 21.6 atoms/nm^2, well below the expected percolation threshold. (Recall that the third layer starts to fill at 20.4 atoms/nm^2.) The transition temperature on the plateau is also well below that expected from the KTN relation. Even if ρ_s is decreased to 50% of its zero-temperature value by excitations, we would expect a transition temperature on the order of 500 mK at a liquid density of 4 atoms/nm^2. Finally, the sharpness of the transition does not change as the system nears the end of the hypothesized coexistence region. This can be seen in Fig. 13. Although the size of the superfluid signal increases as a function of coverage, the width of the transition, as determined from the width of the dissipation peaks at half of the maximum dissipation, does not decrease significantly. In other words, finite-size effects continue to be important at 26 atoms/nm^2, even though the end of the plateau in T_{peak} versus n indicates the boundary of the coexistence region according to the interpretation of Dash.

Interestingly, the expected decrease in the width of the superfluid transition occurs only between 26 atoms/nm^2 and the completion of the third layer at a coverage of 28 atoms/nm^2. This trend stops abruptly at third-layer completion, above which the width at half maximum of the dissipation peaks is about 50 mK. The residual broadening is probably caused by geometric constraints imposed by the exfoliated substrate. We conclude that the third layer is a homogeneous fluid at completion, but not at lower densities.

In summary, the plateau in T_{peak} between 22 and 26 atoms/nm^2 is suggestive of two-phase coexistence, but the data do not conform in detail to the percolation model. The layer does not appear to be a uniform fluid until completion. As in the second-layer case, the interpretation of these data would benefit from further work with nonexfoliated substrates.

2. Fourth layer

The salient features of the fourth-layer data are the plateaus in T_{peak} and $\Delta P(0)$ between 28 and 30 atoms/nm^2. The superfluid dissipation peak decreases in magnitude and increases in width at coverages just above the end of the plateau as shown in Fig. 15. We now consider two possible explanations of the observed behavior.

One possibility is that the plateau is a sign of a two-phase coexistence region like that proposed for the third layer. This is consistent with the results of Clements *et al.*,[14] who find a coexistence region in each of the first three fluid layers (above the two solid layers). The agreement with the percolation model discussed above, however, is worse than was found for the third-layer case. The most important point is that the period shift does not change at all as the plateau is crossed. Accepting 2 atoms/nm^2, the breadth of the observed plateau in T_{peak}, as the width of the coexistence region, we

would expect ΔP to start increasing for coverages above 29 atoms/nm^2. The period shift, however, is independent of coverage between 28 and 30 atoms/nm^2 within the resolution of our measurement. (The filling curve measurements introduced below, which are much less noisy than the data of Figs. 11 and 14, confirm this conclusion.)

The failure of the percolation model alone should not be taken as a definitive argument against phase separation. The percolation threshold of 45% of the self-bound density represents a sweeping assumption made in the absence of any structural information. Even if we ignore the details, however, there is no sign that the ^{4}He added between 28 and 30 atoms/nm^2 percolates, even after the end of the hypothesized coexistence region is reached. There is, for example, no dramatic increase in $T_{\rm peak}$ above 30 atoms/nm^2, and $\Delta P(0)$ actually increases more slowly than it did in the upper part of the third layer.

Another possible origin of the plateau is a structural change in one of the underlying layers. Lauter *et al.*[10] observe evidence for a reconstruction of the second layer of ^{4}He on graphite in the vicinity of third-layer completion. The lattice constant of the second-layer solid increases by about 2%, implying that the density increases by at least 4%, equivalent to approximately 0.3 atoms/nm^2. The actual density change could be greater if the unreconstructed layer has a large number of defects. The increase in the density of the second layer comes at the expense of the fourth, which does not start to fill until the reconstruction is complete. This is consistent with the fact that the ^{4}He added to the film between 28 and 30 atoms/nm^2 does not appear to contribute to superfluidity.

As we observed above, the dissipation peak at the superfluid transition drops and broadens above 30 atoms/nm^2. This feature, seen in Fig. 15, occurs just above the plateau in $\Delta P(0)$ and $T_{\rm peak}$. Apparently, some change in the film modifies the vortex dynamics. Neither of the above proposals provides a simple explanation of this observation. If the plateau were due to a fourth-layer coexistence region, we would expect the width of the dissipation peak to *decrease* as the system entered a uniform fluid phase. Structural changes in underlying layers might affect the vortex diffusivity and hence the superfluid dissipation peak. In this case, however, we would expect to see the dissipation change within the plateau region, where the structural changes occur, and not after it.

We consider the reconstruction of the second layer to be a stronger candidate than phase separation for explaining the plateaus in $\Delta P(0)$ and $T_{\rm peak}$ between 28 and 30 atoms/nm^2. We note, however, that the fourth layer of ^{4}He on graphite is the most extreme example of a layered superfluid that has been studied to date, and so the debate over this coverage region can be expected to continue. The chemical potential step between the third and fourth layers is about 5 K,[12] which is larger than the characteristic energies for superfluidity as well as the binding energy per atom of the self-bound 2D liquid.[22] Given this large change in energy scale, it is not surprising that the growth of superfluidity is interrupted at third-layer completion.

Above 30 atoms/nm^2, the period shift and transition temperature both increase with coverage as shown in Fig. 11. The signal in this coverage range is large enough to invite a comparison with the data of Agnolet *et al.*[7] for ^{4}He films adsorbed on Mylar. The goal here is to establish whether or not there is quantitative agreement with the Kosterlitz-Thouless theory.[47,48] We wish to compare the real and imaginary parts of the superfluid density, which are related to the measured period shift ΔP and the dissipation Q^{-1} by[7]

$$2\frac{\Delta P}{P}=\frac{I_{s0}}{I}\mathrm{Re}[\epsilon^{-1}(\omega)] \tag{3}$$

and

$$\Delta Q^{-1}=Q^{-1}-Q_0^{-1}=\frac{I_{s0}}{I}\mathrm{Im}[\epsilon^{-1}(\omega)]. \tag{4}$$

I_{s0} is the effective moment of inertia of the superfluid in the absence of vortex pairs and I is the total moment of inertia of the cell. Q_0^{-1} is the dissipation of the empty cell. The real and imaginary parts of the superfluid density are $\rho_{s0}\mathrm{Re}[\epsilon^{-1}(\omega)]$ and $\rho_{s0}\mathrm{Im}[\epsilon^{-1}(\omega)]$, where ρ_{s0} is the bare (or microscopic) superfluid density. The measured superfluid density is $\rho_s(T)=\rho_{s0}(T)/\epsilon(\omega)$, where the dielectric constant $\epsilon(\omega)$ incorporates the effects of vortex-pair screening at the experimental frequency ω. The reader may wish to consult Agnolet *et al.*[7] for a further discussion of the Kosterlitz-Thouless theory. For simplicity, we assume that vortices are the only excitations, so that $\rho_{s0}(T)=\rho_s(0)$, the superfluid density at $T=0$.

We need to reduce our data to the forms $\rho_{s0}\mathrm{Re}[\epsilon^{-1}(\omega)]$ and $\rho_{s0}\mathrm{Im}[\epsilon^{-1}(\omega)]$. This is done by noting that I_s is proportional to ρ_s, so that

$$\frac{I_{s0}}{I}=\left(\frac{\partial I_s}{\partial\rho_s}\right)\frac{\rho_{s0}}{I}. \tag{5}$$

Ideally, $\partial I_s/\partial\rho_s$ is equal to the mass sensitivity of the torsional oscillator, $\partial I/\partial\rho$. As discussed above, the tortuosity of the substrate reduces the sensitivity to superfluid mass, so that

$$\left(\frac{\partial I_s}{\partial\rho_s}\right)=(1-\chi)\frac{\partial I}{\partial\rho}. \tag{6}$$

In the case of the period shift, accepting this tortuosity correction is equivalent to assuming that a fraction $1-\chi$ of the superfluid remains locked to the substrate. The interpretation for the dissipation is somewhat more subtle. The physical origin of the dissipation is the drag force on a vortex in the flow field $\vec{v_s}$ of the superfluid relative to the torsional oscillator. Because of the tortuosity of the substrate, $|v_s|$ is not equal to the velocity v of the substrate relative to the laboratory. Hydrodynamically, an average velocity $\langle v_s\rangle$ in the rest frame of the oscillator can be calculated from the momentum imparted to the superfluid by the substrate. One finds

$$\langle v_s\rangle=-(1-\chi)v. \tag{7}$$

It is therefore equivalent to think of the tortuosity correction as a reduction of either the superfluid mass *or* the average superfluid velocity relative to the oscillator. Since we assume that the dissipation is proportional to v_s, this argument sug-

gests that the tortuosity correction of Eq. (6) applies to the calculation of the imaginary part of ρ_s [Eq. (4)] as well as the real part.

In fact, we expect the dissipation to be sensitive to the microscopic velocity profile, which can be calculated only by solving Euler's equation for a particular substrate geometry. This is not possible for an irregular substrate like Grafoil, but we expect regions to exist where the local flow velocity is much larger than $\langle v_s \rangle$. In this case, the tortuosity correction to Eq. (4) leads to an *overestimate* of the imaginary part of ρ_s. Although a more exact approach is not possible, we note that the maximum velocity scale in the system is set by the substrate velocity. Correspondingly, a lower bound for the imaginary part of ρ_s can be obtained by setting the χ factor to zero in Eq. (6). Since the χ factor is ≈ 0.98–0.99 for ^{4}He on Grafoil, this bound is a factor of 50 – 100 smaller than the value of $\rho_{s0}\mathrm{Im}[\epsilon^{-1}(\omega)]$ determined using the full tortuosity correction.

For the purposes of comparison with the Mylar data, we will proceed using the full tortuosity correction for both the period shift and the dissipation. Using the relation $P = 2\pi\sqrt{I/\gamma}$ (γ is the torsion constant) between the resonant period and the moment of inertia, the scale factor in Eqs. (3) and (4) is

$$\frac{I_{s0}}{I} = \frac{2A_s(1-\chi)}{P}\left(\frac{\partial P}{\partial n}\right)\rho_{s0}, \tag{8}$$

where A_s is the surface area of the substrate and n is the coverage. For the Grafoil cell, $A_s = 12.8\ \mathrm{m}^2$, $(\partial P/\partial n) = 0.897$ nsec/μmol, and $P = 1.558$ msec. At the coverage for which we will make the comparison to the Mylar data, 57.2 μmol/m^2, $\chi = 0.981$. (This is smaller than the χ factor of 0.989 ± 0.004 determined at higher coverages. We use the local slope of the period versus coverage curve to compute the χ factor. In the current case, the slope of the superfluid part of this curve is not constant. This observation will be discussed in more detail in the following section.) For the Mylar cell of Agnolet *et al.*,[7] $A_s = 1.95\ \mathrm{m}^2$, $(\partial P/\partial n) = 0.282$ nsec/μmol, $\chi = 0.144$, and $P = 0.784$ msec.[7] Reducing the data according to Eqs. (3) and (4), we obtain the real and imaginary parts of the superfluid density for the two substrates. These are shown in Fig. 17. The dashed line in the lower panel of the figure is the Nelson-Kosterlitz line,[47]

$$\frac{\rho_s(T_c^-)}{T_c} = 8.725\ \ \mu\mathrm{mol\ m^{-2}\ K^{-1}}, \tag{9}$$

which relates the real part of ρ_s to the static transition temperature T_c. Determining T_c requires a full fit to the dynamic theory, which is not the subject of this paper. Usually, T_c falls just below the "knee" in the real part of ρ_s. In this respect, the real parts of the superfluid density for the two substrates, which are shown in the lower panel of Fig. 17, agree reasonably well. The transition on Grafoil is broader than that observed on Mylar.

Since we have used the full tortuosity correction to calculate the imaginary part of ρ_s in Fig. 17, the data shown in the upper panel of the figure are only upper bounds. The tortuosity correction for Mylar is small, and we therefore expect the data for $\rho_{s0}\mathrm{Im}[\epsilon^{-1}(\omega)]$ shown in Fig. 17 to be fairly

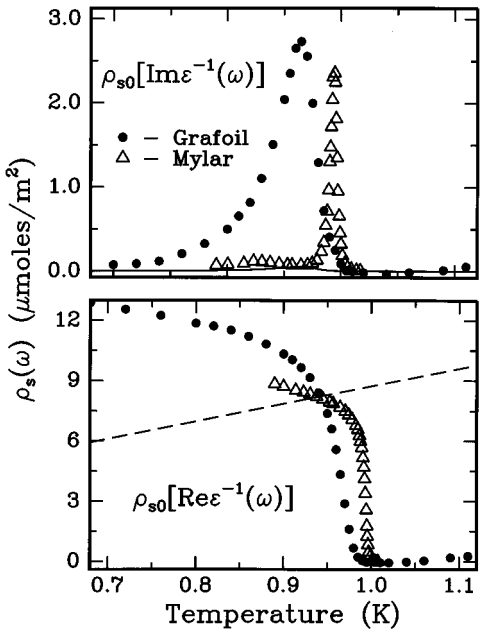

FIG. 17. A comparison of the real (lower panel) and imaginary (upper panel) parts of the superfluid density for ^{4}He films adsorbed on Grafoil (circles) and Mylar (triangles). The Mylar data are from Agnolet *et al.* (Ref. 7). The dashed line in the lower panel is the prediction of Nelson and Kosterlitz for the real part of ρ_s at the transition temperature T_c in the static case ($\omega = 0$). The solid curve in the upper panel is the lower bound on $\rho_{s0}\mathrm{Im}[\epsilon^{-1}(\omega)]$ for ^{4}He-Grafoil (see text). The ^{4}He coverages are 57.2 μmol/m^2 (Grafoil) and 42.5 μmol/m^2 (Mylar).

reliable. For Grafoil, however, the tortuosity factor $\chi \approx 0.98$, and the imaginary part of ρ_s could therefore be up to a factor of 50 smaller than the values shown as solid circles in the figure. We expect the dissipation peak for ^{4}He on Grafoil to be much smaller than for ^{4}He on Mylar and therefore believe that the lower bound, shown in Fig. 17 as a solid curve, is more appropriate. Our reasoning follows that applied by Kotsubo and Williams for the case of a ^{4}He film adsorbed on a spherical surface.[49] Because of the finite surface area of the sphere, the vortex-antivortex pairs which provide the superfluid with its phase stiffness (i.e., superfluid density) do not unbind at some temperature T_c as they do for an infinite surface area at zero frequency. The maximum pair separation is fixed by the diameter of the sphere. The superfluid density decreases to zero, but it does so continuously as more thermally excited vortex pairs, which screen and hence weaken the vortex-antivortex interaction, are created at higher temperatures.

Ideally, the finite sphere diameter has no effect on the size of the real part of the superfluid density $\rho_s(0)$; it only broadens the transition. The effect on the dissipation is much more significant. The dissipation at the Kosterlitz-Thouless transition is dominated by the contribution from vortex pairs with a separation on the order of $r_D = \sqrt{2D/\omega}$, where D is the vortex diffusion constant and ω is the experimental frequency. Adams and Glaberson[50] report a value for D on the order of $\hbar/m$ for films with transition temperatures between 1.3 and 2 K. Using this value, we estimate that r_D in our case is on the order of 10 μm. The superfluid dissipation will be

suppressed if the substrate geometry imposes an upper bound on the vortex separation which is smaller than r_D. For the spherical model, Kotsubo and Williams find that the dissipation maximum decreases by a factor of 5 if $r/r_D \sim 0.2$.

There is no single length scale characterizing our Grafoil substrate. Optical microscopy, however, shows extensive surface damage on a 1 μm length scale. This is smaller than our 10 μm estimate for the diffusion length, indicating that finite-size effects should be important, as confirmed by the broadening of the transition seen in the real part of ρ_s. Dynamic broadening can be ruled out since we are working at a lower frequency than that used in the Mylar experiments. Broadening due to a film-thickness distribution is also unlikely since our films should be more homogeneous than those adsorbed on Mylar. Since finite-size effects should be relevant, we expect the dissipation peak to be smaller than that seen for a film of comparable thickness adsorbed on Mylar.

Unfortunately, quantitative agreement between the imaginary part of ρ_s and the predictions of the dynamic KT model has never been fully established for Mylar,[7] and so it is not clear how much weight should be assigned to Fig. 17. Although ^{4}He on graphite is in some respects an ideal 2D superfluid, the complications introduced by exfoliation may exceed any benefits due to increased local homogeneity. A serious comparison with the Kosterlitz-Thouless theory will require careful experiments on films adsorbed on large single crystals, for which the tortuosity corrections will be much smaller.

VI. HIGHER COVERAGES

A. Results

As can be seen in Fig. 11, another plateau appears in $\Delta P(0)$ in the vicinity of fourth-layer completion. The desorption correction, however, is very significant at these coverages, growing from 0.05 nsec at 35 atoms/nm^2 to 1.5 nsec at 40 atoms/nm^2. The rapid growth is caused by both the rising transition temperature and the increase in the vapor pressure at fourth-layer completion. Since the correction at the highest coverages is of the same order as the superfluid signal, we do not consider the results of the temperature sweeps totally reliable in this regime.

Faced with this shortcoming of the temperature sweeps, we turned to another method to corroborate our results near fourth-layer completion. In the course of accumulating the data for the vapor pressure isotherms at 900 mK, we recorded the resonant period versus coverage, starting from third-layer completion. The resulting *filling curve* is shown in the upper panel of Fig. 18. This figure is a graphic demonstration of the tortuosity effects discussed above. The filling curve of an ideal superfluid film would show a vertical drop at the coverage corresponding to the onset of superfluidity, above which the filling curve should be almost flat.[7] For Grafoil, the onset of superfluidity shows up only as a small break in the slope, indicated in Fig. 18 by an arrow.

Additional structure in the filling curve is evident if the raw data are subtracted from the extrapolation of the nonsuperfluid curve, shown as the solid line in the upper panel Fig. 18. The resulting period shift, shown in the lower panel of Fig. 18, *should* be equivalent to taking a cross section of the temperature sweep data at 900 mK. The large step in ΔP occurs at the onset of superfluidity. Above onset, there are regions where the growth of ΔP with coverage is slightly suppressed.

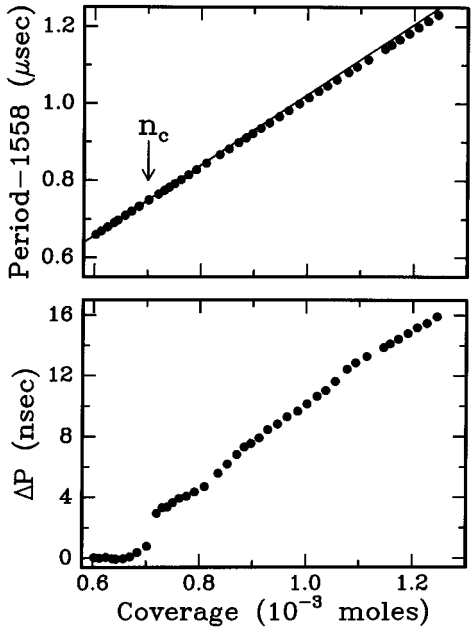

FIG. 18. Filling curve for the Grafoil cell taken at 900 mK is shown in the upper panel. The arrow indicates the onset of superfluidity. The solid line is a fit of the filling curve below onset. The lower panel shows the superfluid period shift ΔP determined by subtracting the data in the upper panel from the fit of the nonsuperfluid data.

Although the data in the lower panel of Fig. 18 are substantially less noisy than those of Fig. 11, the magnitude of the period shift near fourth-layer completion is too large by almost a factor of 2. We decided to attempt a correction by setting the period shift to zero at the onset of superfluidity and then adjusting the slope of the nonsuperfluid curve so that the period shift at fourth-layer completion agreed with that determined from the temperature sweeps. We then proceeded to apply a similar correction procedure to filling curves obtained at 20 mK and 500 mK. (For the latter two curves, the films were not annealed for coverages above the onset of superfluidity. We assumed that the mobility of superfluid film was sufficient to guarantee a uniform coverage.) The three adjusted filling curves are shown in Fig. 19. We reiterate that each of these curves was constructed for a particular slope of the nonsuperfluid filling curve: 0.893 nsec/μmol at 20 mK, 0.898 nsec/μmol at 500 mK, and 0.900 nsec/μmol at 900 mK. This rather *ad hoc* procedure makes us reluctant to assign too much quantitative weight to these data. Nonetheless, each curve shows a plateau near fourth-layer completion, in agreement with the measurements conducted using the temperature sweep technique. Furthermore, the 500 mK and 900 mK curves also show a suppression of the period shift near fifth-layer completion. (The heat load due to superfluid film flow in the fill capillary prevented us from cooling thicker films to 20 mK.)

One might challenge the significance of the filling curves, even at the qualitative level. Among the artifacts that could

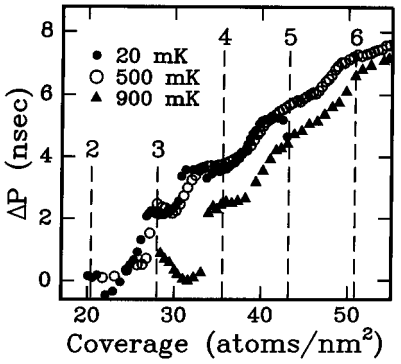

FIG. 19. The period shift ΔP as a function of coverage at temperatures of 20 mk (solid circles), 500 mK (open circles), and 900 mK (triangles). The dashed lines indicate layer completion.

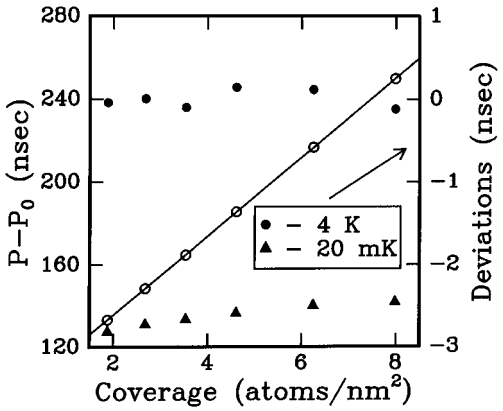

FIG. 20. Filling curve data for first-layer coverages up to 8.5 atoms/nm^2. The open circles are period versus coverage data obtained at 4 K. The solid circles are deviations of the 4 K points from a linear fit to the data. The solid triangles are the difference between the period measured at 20 mK and the linear fit of the 4 K filling curve. The period offset P_0 is 1.558 msec.

affect these measurements are capillary condensation,[51] coupling to third sound,[8] and, particularly for the two low-temperature curves, a nonequilibrium film distribution. Capillary condensation, for example, could trap helium in wedges formed by leaves of graphite, leading to a drop in the signal such as that seen in the 20 mK curve of Fig. 19 near fifth-layer completion. These topics are discussed in more detail in Ref. 36. An important question, for which we cannot provide a definitive answer, is why the nonsuperfluid slopes for each curve are apparently different. Furthermore, in choosing the nonsuperfluid slope to obtain a superfluid period shift of the correct size, we are left with anomalous behavior like that seen for the 900 mK curve in Fig. 3: The period shift is positive and decreases with increasing coverage as the onset of superfluidity at 32 atoms/nm^2 is approached from below. Interestingly, the 500 mK curve shows a small decrease in ΔP in the same coverage range, even though the film is superfluid at this temperature. The 20 mK curve, however, is flat between 28 and 30 atoms/nm^2, consistent with the plateau found in the temperature sweep measurements.

B. Higher coverages: Discussion

The period shift data show plateaus near fourth-, fifth-, and sixth-layer completion, as can be seen in Fig. 19. These plateaus start before layer completion, unlike the plateau between 28 and 30 atoms/nm^2 that was discussed in the previous section. This makes it even less likely that they are due to two-phase coexistence. The two-phase coexistence region is expected to occur at low densities within each layer.[52] Unless there is a large spread in film thickness, we would not expect to see any signature of the coexistence region before layer completion.

Another idea is that the plateaus are due to modulations of the superfluid density in a uniform fluid film. This approach has been considered in recent path-integral Monte Carlo simulations by Zimanyi *et al.*[53] These authors considered the effect of the He-He repulsion on the *microscopic* superfluid density ρ_s of the film. As ^{4}He atoms are added to a single layer of the film, the hard-core repulsion becomes increasingly important. The repulsion competes with the exchange interaction, which favors superfluidity. If the exchange is sufficiently weak, the repulsive interactions drive the system towards ''Bose-insulating'' behavior as the layer approaches completion. Below a critical exchange strength, the film will be totally localized (i.e., nonsuperfluid) at layer completion.[54] For stronger exchange, the superfluid density will be supressed near layer completion but will remain nonzero.

This model, which is extended by Zimanyi *et al.* to multilayer films, predicts that ρ_s will increase less rapidly as a layer approaches completion, in agreement with the experimental data. We emphasize that the model allows for an explicit calculation of the superfluid density ρ_s as opposed to assuming that ρ_s is simply proportional to the areal liquid density n (an assumption implicit throughout most of this paper). These advantages come at a cost: The real He-He interaction is replaced by a hard-core potential and the ^{4}He-substrate interaction is included only in a self-consistent fashion. The appearance of phase separation in the calculation of Clements *et al.*,[13] which uses more realistic potentials, thus indicates that caution is appropriate. An explicit calculation of the superfluid density within a more realistic framework would play a helpful role in resolving this debate.

VII. FIRST $1\frac{1}{2}$ LAYERS

Our study of the first $1\frac{1}{2}$ layers is less complete than for higher coverages. The most useful data are in the form of filling curve measurements, obtained in a manner similar to that used for higher densities except that the coverages were annealed and cooled according to the guidelines of Table I. In no case did we find an indication of superfluidity. We did not, however, perform a complete set of temperature sweep measurements. Furthermore, we have no data for the region between 8 and 13 atoms/nm^2.

A. First layer

Filling curve data for six coverages below 8 atoms/nm^2 are shown in Fig. 20. The open circles in this figure show the raw filling curve data at 4 K. The solid circles show the *deviations* of these data from a linear fit. The deviations fall

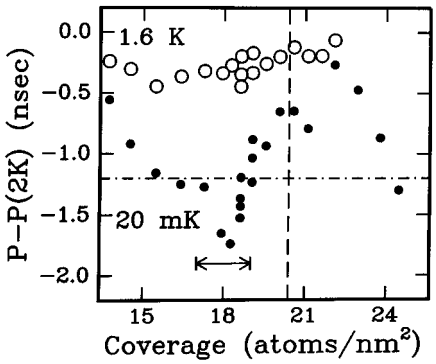

FIG. 21. The difference between the period at 1.6 K and the filling curve measured at 2.0 K is shown using open circles for coverages between 13 and 25 atoms/nm^2. The difference between the period at 20 mK and the 2.0 K filling curve is shown using solid circles. The vertical dashed line indicates second-layer completion and the horizontal line indicates the empty-cell value of $P(0.020\ \mathrm{K})-P(2.0\ \mathrm{K})$. The double arrow brackets the region of second-layer superfluidity.

on a horizontal line with a scatter of about 0.2 nsec and no systematic error. The triangles in Fig. 20 show the difference between the filling curve measured at 20 mK and the linear fit of the 4 K filling curve. These data form a nearly horizontal line, parallel to the deviations at 4 K. (There is a slight drop of the 20 mK curve at low coverages, but this is smaller than the noise in the 4 K filling curve.) The filling curves at 4 K and 20 mK thus differ only by a constant and superfluidity is therefore absent within the resolution of our measurement.

B. Second layer

The filling curve data for coverages between 13 and 25 atoms/nm^2 are shown in Fig. 21, which comprises two traces. The upper curve is the difference $P(1.6\ \mathrm{K})-P(2.0\ \mathrm{K})$ between the period at 1.6 K and a linear fit of the filling curve measured at 2.0 K. In fitting the 2 K filling curve, we have used only the data from below second-layer completion since desorption becomes significant at higher coverages. The difference $P(1.6\ \mathrm{K})-P(2.0\ \mathrm{K})$ is a horizontal line with scatter of ± 0.2 nsec, as expected for the difference of two filling curves in the absence of superfluidity. The lower curve in Fig. 21 is the difference $P(0.020\ \mathrm{K})-P(2.0\ \mathrm{K})$, and the horizontal dotted line is the value of $P(0.020\ \mathrm{K})-P(2.0\ \mathrm{K})$ for the empty cell. [The empty-cell background covered only a temperature range from 20 mK to 1.6 K. The difference $P(0.020\ \mathrm{K})-P(2.0\ \mathrm{K})$ is inferred from the empty-cell value of $P(0.020\ \mathrm{K})-P(1.6\ \mathrm{K})$ and a zeroth-order fit of the second-layer data for $P(1.6\ \mathrm{K})-P(2.0\ \mathrm{K})$.] The large dip in the 20 mK data near 18 atoms/nm^2 corresponds to the superfluid phase in the second layer. The drop above 22 atoms/nm^2 is due to the onset of superfluidity in the third layer. The surprising aspect of these data is that the period at 20 mK is *above the background* for coverages just above first- and second-layer completion. This effect, which we found to be reproducible upon warming and cooling again, is opposite in sign to that expected for superfluidity. Since the effect is most prominent just above promotion into the second and third layers, it is possible that phase separation is playing a role. It is not apparent, however, how phase separation should *increase* the effective moment of inertia of the cell. These observations merit more careful study over a finer coverage grid with an accompanying set of temperature sweep measurements.

VIII. CONCLUSIONS

The results discussed in this paper establish that superfluidity in ^{4}He films adsorbed on graphite is distinct from that observed on disordered substrates. Structural phase transitions in the film have a significant impact on its superfluid properties. Superfluidity in the second layer is suppressed by the solidification of the film. Two-phase coexistence plays a role in the third layer, where we observe a plateau in the superfluid transition temperature over most of the layer. A second plateau at low coverages in the fourth layer probably originates in the reconstruction of one of the underlying layers. At higher coverages, the layer-by-layer growth of the film modulates the superfluid period shift out to the completion of the sixth layer. The data for the first 1.5 layers show no indication of superfluidity, but some anomalous features in the filling curve measurements will need to be addressed in future experiments.

There is no shortage of possible experiments to study further the ^{4}He-graphite system. We have not yet examined the first 1.5 layers over a fine grid of temperature and coverage. We anticipate that small modifications in cell design will lead to the elimination of the 300 mK anomaly that prevented more accurate period shift measurements in the second-layer superfluid regime. Perhaps the most valuable step, however, will be the study of superfluidity on nonexfoliated substrates. The loss of surface area need not be prohibitive. The tortuosity factor will be much smaller than for Grafoil and significantly larger crystalline domain sizes can be achieved.

Many of the results presented in this paper should not be specific to the ^{4}He-graphite system. Phase separation, for example, should accompany layering transitions for ^{4}He adsorbed on other substrates.[13] Of particular interest in this regard is crystalline H_2, on which ^{4}He is much less strongly bound than on graphite and superfluidity occurs in the first monolayer of adsorbed helium.[55] In many respects, the first layer of ^{4}He on H_2 should be similar to the third layer on graphite, except that the effects of substrate corrugation should be stronger. Recent third sound experiments by Chen *et al.* show the propagation of a second collective mode in submonolayer ^{4}He on H_2,[56] an observation that has led to considerable theoretical speculation about the role of substrate corrugation.[42,57] It would be very useful to conduct a set of torsional oscillator measurements, expanding on the work of Adams and Pant[58] at higher coverages, in the coverage regime of the third sound study of Chen *et al.*[56] A comparison of the ^{4}He-graphite and ^{4}He-H_2 systems would be the first step in identifying the universal aspects of superfluidity on ordered substrates.

ACKNOWLEDGMENTS

We are grateful for the continuing interest of Moses Chan in this work. We also wish to acknowledge useful discus-

sions with N.W. Ashcroft, B. Clements, V. Elser, H. Godfrin, D.S. Greywall, and E. Siggia and thank Geoff Zassenhaus for his assistance in preparing the figures and the manuscript. P.A.C. acknowledges financial support from AT&T Bell Laboratories. This work was supported by the National Science Foundation under Grant No. DMR-8921733 and by the MRL program of the National Science Foundation under Award No. DMR-91-21654.

*Present address: Department of Physics, University of California, Santa Barbara, CA 93106.

[1] J.M. Kosterlitz and D.J. Thouless, J. Phys. C **5**, L124 (1973); **6**, 1181 (1973).
[2] D.J. Bishop and J.D. Reppy, Phys. Rev. Lett. **40**, 1727 (1978); I. Rudnick, *ibid.* **40**, 1454 (1978).
[3] M. Bretz, J.G. Dash, D.C. Hickernell, E.O. McLean, and O.E. Vilches, Phys. Rev. A **8**, 1589 (1973).
[4] D.S. Greywall, Phys. Rev. B **47**, 309 (1993).
[5] M. Chester and L.C. Yang, Phys. Rev. Lett. **31**, 1377 (1973).
[6] D.J. Bishop, J.E. Berthold, J.M. Parpia, and J.D. Reppy, Phys. Rev. B **24**, 5047 (1981).
[7] G. Agnolet, D.F. McQueeney, and J.D. Reppy, Phys. Rev. B **39**, 8934 (1989).
[8] G. Zimmerli, G. Mistura, and M.H.W. Chan, Phys. Rev. Lett. **68**, 60 (1992).
[9] P.A. Crowell and J.D. Reppy, Phys. Rev. Lett. **70**, 3291 (1993); Physica B **197**, 269 (1994).
[10] H.J. Lauter, H. Godfrin, V.L.P. Frank, and P. Leiderer, in *Phase Transitions in Surface Films 2*, edited by H. Taub *et al.* (Plenum, New York, 1991).
[11] R.L. Elgin and D.L. Goodstein, Phys. Rev. A **9**, 2657 (1974).
[12] D.S. Greywall and P.A. Busch, Phys. Rev. Lett. **67**, 3535 (1991).
[13] B.E. Clements, E. Krotscheck, and H.J. Lauter, Phys. Rev. Lett. **70**, 1287 (1993); B.E. Clements, J.L. Epstein, E. Krotscheck, and M. Saarela, Phys. Rev. B **48**, 7450 (1993); B.E. Clements, H. Forbert, E. Krotscheck, and M. Saarela, J. Low Temp. Phys. **95**, 849 (1994).
[14] *Phase Transitions in Surface Films*, edited by J.G. Dash and J. Ruvalds (Plenum, New York, 1980); *Phase Transitions in Surface Films 2*, edited by H. Taub, G. Torzo, H.J. Lauter, and S.C. Fain, Jr. (Plenum, New York, 1991).
[15] M. Schick, in *Phase Transitions in Surface Films*, edited by J.G. Dash and J. Ruvalds (Plenum, New York, 1980).
[16] S.V. Hering, S.W. Van Sciver, and O.E. Vilches, J. Low Temp. Phys. **25**, 793 (1976).
[17] S.E. Polanco and M. Bretz, Phys. Rev. B **17**, 151 (1978).
[18] M. Bretz, in *Monolayer and Submonolayer Helium Films*, edited by J.G. Daunt and E. Lerner (Plenum, New York, 1973).
[19] D.S. Greywall, Phys. Rev. B **41**, 1842 (1990); V. Elser, Phys. Rev. Lett. **62**, 2405 (1989).
[20] J.G. Dash, *Films on Solid Surfaces* (Academic Press, New York, 1975).
[21] R.E. Ecke, Q.S. Shu, T.S. Sullivan, and O.E. Vilches, Phys. Rev. B **31**, 448 (1985).
[22] P.A. Whitlock, G.V. Chester, and M.H. Kalos, Phys. Rev. B. **38**, 2418 (1988).
[23] J.M. Gottlieb and L.W. Bruch, Phys. Rev. B **41**, 7195 (1990); **48**, 3943 (1993).
[24] A.N. Berker and D.R. Nelson, Phys. Rev. B **19**, 2488 (1979); J. Tobochnik and G.V. Chester, *ibid.* **20**, 3761 (1979).
[25] D.M. Ceperley and E.L. Pollock, Phys. Rev. B **39**, 2084 (1989).
[26] J.A. Herb and J.G. Dash, Phys. Rev. Lett. **29**, 1846 (1972).
[27] S.E. Polanco and M. Bretz, Surf. Sci. **94**, 1 (1980).
[28] K.R. Atkins, Phys. Rev. **113**, 962 (1959).
[29] J.A. Roth, G.J. Jelatis, and J.D. Maynard, Phys. Rev. Lett. **44**, 333 (1980).
[30] G.K.S. Wong, P.A. Crowell, H.A. Cho, and J.D. Reppy, Phys. Rev. B **48**, 3858 (1993).
[31] Grafoil and UCAR graphite foam are manufactured by the Union Carbide Corporation.
[32] R.J. Birgeneau, P.A. Heiney, and J.P. Pelz, Physica B **109** & **110**, 1785 (1982).
[33] D.J. Bergman, B.I. Halperin, and P.C. Hohenberg, Phys. Rev. B **11**, 4253 (1975).
[34] K.A. Shapiro and I. Rudnick, Phys. Rev. **137**, A1383 (1965).
[35] J.A. Roth, T.P. Brosius, and J.D. Maynard, Phys. Rev. B **38**, 11209 (1988).
[36] P.A. Crowell, Ph.D. thesis, Cornell University, 1994.
[37] B. Yurke, Ph.D. thesis, Cornell Unviersity, 1983.
[38] DuPont Electronics, HPF Customer Services, Wilmington, DE 19880.
[39] MKS Instruments, 6 Shattuck Road, Andover, MA 01810.
[40] Y. Larher, J. Chem. Phys. **68**, 2257 (1978).
[41] G.G. Batrouni, R.T. Scalettar, G.T. Zimanyi, and A.P. Kampf, Phys. Rev. Lett. **74**, 2527 (1995).
[42] K. Mullen, H.T.C. Stoof, M. Wallin, and S.M. Girvin, Phys. Rev. Lett. **72**, 4013 (1994).
[43] A.F. Andreev and I.M. Lifshitz, Sov. Phys. JETP **29**, 1107 (1969); G.V. Chester, Phys. Rev. A **2**, 256 (1970); I.E. Dzyaloshinskii *et al.*, Sov. Phys. JETP **35**, 823 (1972); I.E. Dzyaloshinskii *et al.*, *ibid.* **35**, 1213 (1972).
[44] M.W. Meisel, Physica B **178**, 121 (1992).
[45] S.N. Coppersmith, D.S. Fisher, B.I. Halperin, P.A. Lee, and W.F. Brinkman, Phys. Rev. B **25**, 349 (1982).
[46] J.G. Dash, Phys. Rev. Lett. **41**, 1178 (1978).
[47] D.R. Nelson and J.M. Kosterlitz, Phys. Rev. Lett. **39**, 1201 (1977).
[48] B.A. Huberman, R.J. Myerson, and S. Doniach, Phys. Rev. Lett. **40**, 780 (1978); V. Ambegaokar, B.I. Halperin, D.R. Nelson, and E.D. Siggia, Phys. Rev. B **21**, 1806 (1980).
[49] V. Kotsubo and G. Williams, Phys. Rev. B **33**, 6106 (1986).
[50] P.W. Adams and W.I. Glaberson, Phys. Rev. B **35**, 4633 (1987).
[51] M.J. Lysek, M.A. LaMadrid, P.K. Day, and D.L. Goodstein, Phys. Rev. B **47**, 7389 (1993); D.L. Goodstein (private communication).
[52] Clements *et al.* (Ref. 13) find a layering transition near 6.8 atoms/nm^2 in their model, somewhat smaller than the accepted value (7.6 atoms/nm^2) for the density of the third layer.
[53] G.T. Zimanyi, P.A. Crowell, R.T. Scalettar, and G.G. Batrouni, Phys. Rev. B **50**, 6515 (1994).
[54] M.P.A. Fisher, P.B. Weichman, G. Grinstein, and D.S. Fisher, Phys. Rev. B **40**, 546 (1989).
[55] P.J. Shirron and J.M. Mochel, Phys. Rev. Lett. **67**, 118 (1991).
[56] M.-T. Chen, J.M. Roesler, and J.M. Mochel, J. Low Temp. Phys. **89**, 125 (1992); J.M. Mochel and M.-T. Chen, Physica B **197**, 278 (1994).
[57] M. Wagner and D.M. Ceperley, J. Low Temp. Phys. **94**, 185 (1994).
[58] P.W. Adams and V. Pant, Phys. Rev. Lett. **68**, 2350 (1992).